High-density polarization-induced 2D electron gases in N-polar pseudomorphic undoped GaN/$Al_{0.85}Ga_{0.15}N$ heterostructures on single-crystal AlN substrates

Cite as: Appl. Phys. Lett. **121**, 082107 (2022); doi: 10.1063/5.0107159
Submitted: 2 July 2022 · Accepted: 11 August 2022 ·
Published Online: 25 August 2022

Zexuan Zhang,[1,a)] Jimy Encomendero,[1] Eungkyun Kim,[1] Jashan Singhal,[1] YongJin Cho,[1] Kazuki Nomoto,[1] Masato Toita,[2] Huili Grace Xing,[1,3,4] and Debdeep Jena[1,3,4]

AFFILIATIONS

[1]School of Electrical and Computer Engineering, Cornell University, Ithaca, New York 14853, USA
[2]Advanced Devices Technology Center, Asahi Kasei Corporation, Hibiya Mitsui Tower, 1-1-2 Yurakucho, Chiyoda-ku, Tokyo 100-8440, Japan
[3]Department of Materials Science and Engineering, Cornell University, Ithaca, New York 14853, USA
[4]Kavli Institute at Cornell for Nanoscale Science, Ithaca, New York 14853, USA

[a)]Author to whom correspondence should be addressed: zz523@cornell.edu

ABSTRACT

The polarization difference and band offset between Al(Ga)N and GaN induce two-dimensional (2D) free carriers in Al(Ga)N/GaN heterojunctions without any chemical doping. A high-density 2D electron gas (2DEG), analogous to the recently discovered 2D hole gas in a metal-polar structure, is predicted in a N-polar pseudomorphic GaN/Al(Ga)N heterostructure on unstrained AlN. We report the observation of such 2DEGs in N-polar undoped pseudomorphic GaN/AlGaN heterostructures on single-crystal AlN substrates by molecular beam epitaxy. With a high electron density of $\sim 4.3 \times 10^{13}/cm^2$ that maintains down to cryogenic temperatures and a room temperature electron mobility of $\sim 450\ cm^2/V\ s$, a sheet resistance as low as $\sim 320\ \Omega/\square$ is achieved in a structure with an 8 nm GaN layer. These results indicate significant potential of AlN platform for future high-power RF electronics based on N-polar III-nitride high electron mobility transistors.

Published under an exclusive license by AIP Publishing. https://doi.org/10.1063/5.0107159

High density two-dimensional hole gases (2DHGs) induced by the negative polarization charge at the heterointerfaces were discovered recently in metal-polar pseudomorphic undoped GaN/AlN heterostructures on AlN templates and bulk substrates.[1,2] The high conductivity of 2DHGs in these structures led to the first nitride p-channel transistors that break the GHz speed barrier ($f_T/f_{max} \sim 20$ GHz) and currents exceeding 400 mA/mm.[3] Compared to AlN templates, single-crystal AlN substrates offer advantages such as higher hole mobility due to the much lower dislocation densities and the absence of thermal boundary resistance.[2,4]

In contrast to the metal-polar 2DHG structure, in a N-polar pseudomorphic GaN/Al(Ga)N heterojunction on unstrained AlN, the net polarization charge becomes positive in sign and should induce electrons, which are further confined by the band offset between GaN and Al(Ga)N to form a two-dimensional electron gas (2DEG). Such 2DEGs are scientifically and technologically relevant as they can be used as channels for high electron mobility transistors (HEMTs), which simultaneously take advantage of the high electrical resistivity (bandgap > 6 eV) and thermal conductivity ($\sim$340 W/m K) of AlN as well as some merits of N-polar structures such as simpler formation of low-resistance contacts.[5,6] Moreover, the realization of both electron and hole gases in the same GaN/Al(Ga)N structures with opposite polarity offers the opportunity for monolithic integration of complementary logic on AlN using lateral polarity structures.[7] However, the experimental observation of such 2DEGs has never been reported to date.

In this work, we report the observation of polarization-induced 2DEGs in undoped pseudomorphic N-polar GaN/$Al_{0.85}Ga_{0.15}N$ heterostructures on free-standing N-polar AlN substrates. A series of three samples with GaN channel thicknesses of 5, 8, and 10 nm are studied. Temperature-dependent Hall effect measurements confirm the presence of polarization-induced 2DEGs in all these structures.

An electron density as high as $\sim 4.3 \times 10^{13}/\text{cm}^2$, thanks to the high Al-content in the AlGaN back barrier, and a room temperature electron mobility of $\sim 450\,\text{cm}^2/\text{V s}$ are achieved in a structure with 8 nm GaN channel, leading to a low sheet resistance of $\sim 320\ \Omega/\square$. Though no significant difference was seen in the transport properties of 2DEGs between structures with 10 and 8 nm GaN channels, a 36% drop in room temperature electron mobility was observed when the channel thickness decreased to 5 nm.

We use plasma-assisted molecular beam epitaxy (MBE) for the study of the 2DEGs in this work, though the results are thought to be achievable by other growth techniques. The MBE growth of the studied structures was performed in a Veeco GEN10 MBE system equipped with standard effusion cells for Ga and Al and a radio frequency plasma source for active N species. KSA Instruments reflection high-energy electron diffraction (RHEED) apparatus with a Staib electron gun operating at 15 kV and 1.5 A was used to *in situ* monitor the growth front. The substrates used in this study are free-standing N-polar AlN bulk substrates with a dislocation density $<10^4/\text{cm}^2$ from Asahi-Kasei Corporation.[8] After *ex situ* cleaning in acetone, isopropyl alcohol, and de-ionized water (each for 10 min), diced $7 \times 7\,\text{mm}^2$ AlN substrates were mounted in indium-free holders, loaded into the MBE system, and outgassed at 200 °C for 8 h.

Prior to the growth of epi-layers, *in situ* Al-assisted surface cleaning,[9,10] similar to that developed for N-polar AlN templates,[11] was first performed in the MBE growth chamber to remove native oxides and other chemical impurities, which would otherwise lead to polarity inversion and defect generation during epitaxy, from the highly reactive N-polar AlN surfaces. The substrate was heated up to a thermocouple temperature of ~1100 °C and then exposed to an aluminum flux of 20 nm/min for 30 s. The Al shutter was closed long enough for the deposited Al to desorb (monitored by the saturation of RHEED intensity). Such process of Al adsorption and desorption was repeated for 100 cycles, and almost no difference was observed in the evolution of RHEED intensity vs time during the last few cycles, indicative of surface being sufficiently cleaned. This Al-assisted surface cleaning has been found to be critical for the MBE grown epilayer to inherit and maintain the N-polarity of the substrate and not flip to metal-polarity.[11,12]

After the Al-assisted cleaning, a 1000 nm AlN layer was first grown at a thermocouple temperature of ~1080 °C with the Al beam equivalent pressure (BEP) of 7.5×10^{-7} Torr and nitrogen plasma operating at 400 W with the N_2 gas flow rate of 1.85 sccm. Similar growth condition was found to produce smooth N-polar AlN films on single-crystal AlN substrates.[12] After desorbing the excess Al droplets *in situ* at an elevated temperature of ~1180 °C, the substrate was cooled down to ~900 °C for the deposition of 50 nm undoped $Al_{0.85}Ga_{0.15}N$ layer under metal-rich condition. Following the desorption of excess Ga droplets accumulated during the AlGaN growth, a t nm GaN layer (t = 5, 8, and 10) was finally deposited under Ga-rich condition at ~810 °C. The substrate was held long enough at the GaN growth temperature to desorb excess Ga droplets before cooling down to room temperature. A schematic of the epitaxial structures is shown in Fig. 1(a). The purpose of the AlGaN layer between AlN and GaN is to prevent unwanted silicon impurities "floating" on the growth front of the AlN under the Al-rich growth condition from reaching and scattering electrons at the GaN/Al(Ga)N heterojunction where the 2DEG is desired and, hence, improve the 2DEG mobility.[13] 2DEGs in

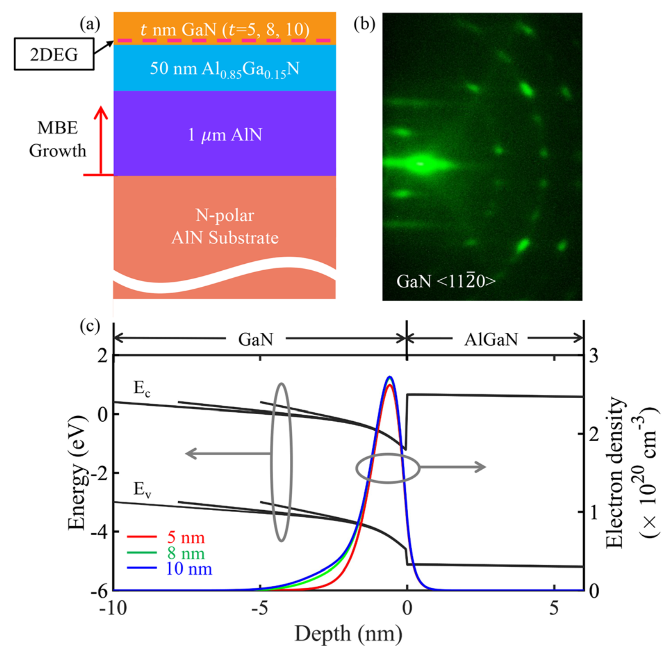

FIG. 1. (a) Schematic of the epitaxial structures in this study. (b) RHEED pattern of GaN surface covered by Ga droplets viewed along ⟨11$\bar{2}$0⟩ azimuth at ~200 °C. (c) Simulated band diagrams and electron density at GaN/AlGaN interface with a surface barrier height of ~0.3 eV.

N-polar AlN/GaN binary alloy heterojunctions without the insertion of AlGaN layers would be presented as a separate study.

RHEED reconstruction of GaN surfaces provides a direct determination of crystal polarity. Specifically, with Ga coverage and at low temperatures (below 300 °C), metal-polar GaN surfaces show "1×1" reconstruction, whereas 3×3, 6×6, and c(6×12) reconstructions have been reported for N-polar GaN surfaces.[14,15] In order to determine the polarity of the epi-structures by RHEED reconstruction, a separate sample was prepared with similar structure as shown in Fig. 1(a) except that the excess Ga droplets after GaN growth were not desorbed to ensure Ga coverage on the surface. Fig. 1(b) shows the RHEED pattern of this sample viewed along GaN ⟨11$\bar{2}$0⟩ azimuth at ~200 °C. A clear c(6×12) reconstruction was observed, confirming the N-polarity of the structures. In addition, KOH etching was also applied to identify the polarity. The appearance of hexagonal pyramids (not shown) after etching in KOH corroborated that the epi-structures are N-polar.

Figure 1(c) shows the simulated energy band diagrams and electron densities at the GaN/AlGaN interfaces for structures with varying GaN channel thickness using a self-consistent 1D Schrödinger–Poisson solver, assuming a surface barrier height of ~0.3 eV for N-polar GaN[16,17] and a zero electric field deep inside the bulk AlN. Other material parameters used for simulation are listed in the supplementary material Table SI. Although the energy band diagram simulation also suggests another parallel 2DEG channel (with much lower electron concentration) at the bottom AlGaN/AlN interface (not shown), we did not observe any measurable conductivity (sheet resistance > 1 MΩ) in a control sample with similar epitaxial structure

Published under an exclusive license by AIP Publishing

as Fig. 1(a) without the topmost GaN layer. This indicates that the carrier transport (as discussed later) in samples shown in Fig. 1(a) is entirely by the 2DEGs formed at GaN/AlGaN interfaces. The very high sheet resistance of the control sample is likely due to the localization of these carriers in deep levels.

The structural properties of the epitaxial structures were characterized by x-ray diffraction (XRD) using a PANalytical Empyrean setup at 45 kV and 40 mA with Cu Kα1 radiation (1.5406 Å). Clearly resolved thickness fringes were observed in the symmetric $2\theta/\omega$ XRD scans in Fig. 2(a) of all the three samples in this study, indicating abrupt hetero-interfaces. The reciprocal space maps (RSMs) around the asymmetric (105) diffractions of GaN, AlGaN, and AlN of all the samples further suggest that both the GaN and AlGaN layers are fully strained to the underlying AlN. Figure 2(b) shows an example with 8 nm GaN.

The surface morphologies of the samples were measured using atomic force microscopy (AFM) in an Asylum Research Cypher ES setup. The 10×10 μm^2 AFM scan of the as-grown surface with 8 nm GaN shows a smooth morphology with no spiral hillocks and a low root mean square (rms) roughness of 0.8 nm, as shown in Fig. 2(c). In addition, the zoomed in 2×2 μm^2 scan [Fig. 2(d)] reveals parallel atomic steps, suggesting a step-flow growth mode. Similar surface morphologies were also observed on the two other samples with different GaN thicknesses.

Hall-effect measurements in van der Pauw geometry were performed using indium dots as Ohmic contacts at a magnetic field of 1 T to study the transport properties of the 2DEGs in these structures. Figure 3(a) shows the measured room temperature (red filled squares) and 77 K (blue empty squares) electron density as a function of channel thickness along with the simulated 2DEG density at the GaN/AlGaN interfaces (gray dashed line) using a self-consistent 1D Schrödinger–Poisson solver with a surface barrier height of 0.3 eV.[16,17] The agreement between the measured and simulated 2DEG densities at the GaN/AlGaN interfaces suggests that the charge transport in these heterostructures is dominated by the GaN/AlGaN 2DEGs. The density of the 2DEGs remains almost unchanged down to cryogenic temperatures, consistent with the polarization-induced origin. Figure 3(b) shows the measured 300 (red circles) and 77 K (blue circles) electron mobilities vs channel thickness. While no significant change in electron mobility (difference <3% at 300 K) was observed when the channel thickness decreased from 10 to 8 nm, a degradation of electron mobility was seen upon decreasing the GaN channel thickness to 5 nm.

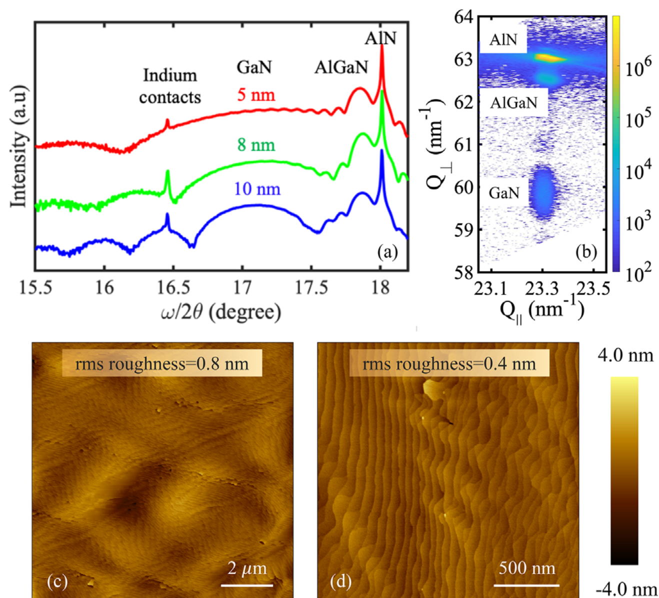

FIG. 2. (a) Symmetric $2\theta/\omega$ XRD scans across (002) diffractions. The peaks marked as indium contacts are from the indium dots placed on sample corners for transport measurements. (b) RSM across the asymmetric (105) diffractions for the 8 nm GaN sample. (c) 10×10 μm^2 AFM micrograph of the as-grown surface with rms roughness ~0.8 nm. (d) 2×2 μm^2 AFM micrograph showing parallel atomic steps. The AFM micrographs were taken on the 8 nm GaN sample.

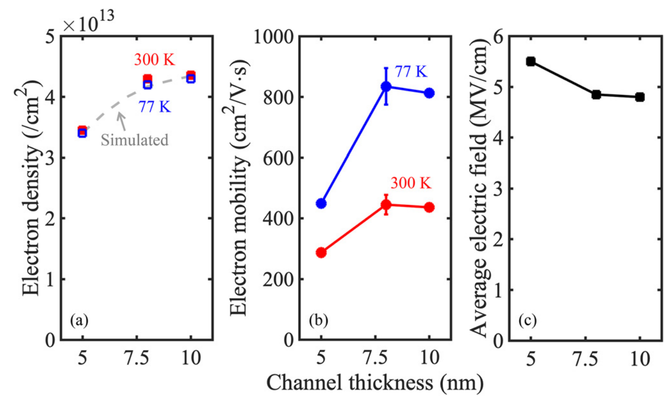

FIG. 3. (a) Room-temperature (red filled squares) and 77 K (blue empty squares) 2DEG density as a function of channel thickness. (b) Room temperature (red) and 77 K (blue) electron mobility vs channel thickness. (c) Average electric field experienced by 2DEG calculated from Schrödinger–Poisson simulation as a function of channel thickness.

A similar decrease in electron mobility when the channel thickness is scaled down has been reported in N-polar GaN/AlGaN structures on unstrained GaN buffer layers. It is attributed to the stronger interface scattering as electrons are pushed closer to the interface by the increased electric field in the channel.[18,19] The average electric field experienced by electrons $F_{avg} = \frac{\int n(z)F(z)\,dz}{\int n(z)\,dz}$, where $n(z)$ is the local electron density and $F(z)$ is the local electric field calculated from the self-consistent 1D Schrödinger–Poisson simulation. This field which is plotted as a function of channel thickness in Fig. 3(c). Indeed, a drop in average electric field is seen as the channel thickness increases from 5 to 8 nm, whereas the difference is quite small between 8 and 10 nm cases. It is worth noting that unlike on unstrained GaN buffer layers, a further increase in GaN channel thickness on AlN substrates will eventually lead to strain relaxation due to the lattice mismatch between GaN and AlN.[20] Understanding the role of strain relaxation on carrier transport in structures with thicker GaN layers will be a future direction. We also note that the 2DEGs in the pseudomorphic N-polar heterostructures on AlN studied here exhibit ~3–4× lower mobilities, but ~3–4× higher 2DEG densities than those on GaN substrates.

To understand the limiting scattering mechanisms, temperature dependent Hall-effect measurements were performed on the samples

Published under an exclusive license by AIP Publishing

with 5 and 8 nm GaN channels. The red and green circles in Fig. 4 show the measured electron mobility in the structures with 5 [Fig. 4(a)] and 8 nm [Fig. 4(b)] GaN channels, respectively. The electron mobility increases monotonically upon lowering the temperature, as expected due to freeze out of phonon scattering. The solid black lines in Fig. 4 represent the calculated electron mobility by combining the contributions from each scattering mechanisms (shown by the gray dashed lines) using Matthiessen's rule. The material parameters used for mobility calculations are listed in supplementary material Table SI. The lattice parameters are extracted from the reciprocal space map shown in Fig. 2(b), whereas the other parameters such as the acoustic deformation potential, sound velocity, and optical phonon energy are from the literature for unstrained GaN. The impact of strain on these parameters is considered to be weak and not included in the calculations. For example, for optical phonon scattering, the dominant phonon scattering mechanism in the temperature range where phonon scattering is significant, an optical phonon energy of ~93.5 meV is measured on the sample with 8 nm GaN using Raman spectroscopy. Replacing the optical phonon energy of 92 meV for unstrained GaN (supplementary material Table SI) with the measured value leads to a ~6% increase in the optical phonon limited mobility and a ~2% increase in the total mobility for the 8 nm GaN sample at 290 K, which is negligible. More accurate calculations with the effect of strain taken into account will be future directions. Mobility limited by interface roughness scattering (μ_{IR}) was calculated using the model developed in Refs. 19 and 21, which takes into account the effect of electric field in the channel. Other scattering mechanisms such as dislocation scattering and alloy scattering were also considered but were found to be much weaker than those shown in the figure.

Note that because of the heavily degenerate 2DEG concentration, the Hall factor is unity, and the calculated field effect mobility can be compared directly with the Hall-effect mobility. With a correlation length Λ of 1.25 nm (as has been widely used for most III-nitride heterojunctions[34,35]) and a rms roughness parameter Δ of ~0.45 nm, reasonable agreement between the calculated values and experimental data are achieved for both samples. The fact that the temperature-dependent electron mobility for both samples can be fitted with the same set of roughness parameters clearly indicates that the large gap in electron mobility between the 5 and 8 nm GaN samples is not a result of difference in interface quality but is due to the electric field in the channel. Future changes in the layer structure design to decrease channel electric field and growth optimization to reduce interface roughness will be of great importance to boost the electron mobility, where desired.

The monotonic increase in electron mobility with decreasing temperature and the nearly temperature-independent electron density led to a decrease in sheet resistance as the temperature was lowered. For example, the sheet resistance drops from ~320 Ω/□ at room temperature to ~170 Ω/□ at 10 K in the sample with 8 nm GaN.

Figure 5 shows the room temperature electron density and mobility for the three samples in this study together with some of the best reported data in the literature with 2DEGs achieved in both metal-polar (+c) and N-polar (−c) III-nitride semiconductor heterostructures on unstrained GaN or AlN. The metal-polar structures included in the figure are AlGaN/GaN, AlGaN/AlN/GaN, and AlN/GaN on GaN[22–27] and AlN/GaN on AlN,[28–31] whereas the N-polar structures are GaN/AlGaN, GaN/AlN/AlGaN, and GaN/AlN digital alloy on GaN[17,19,32,33] and GaN/AlGaN on AlN in this work. Compared with N-polar structures on unstrained GaN buffer layers (blue filled circles),[17,19,32,33] a higher electron density is obtained in this work on AlN substrates (red filled circles), thanks to the higher Al-content in the AlGaN back barrier. Meanwhile, a comparable sheet resistance of ~300 Ω/□ is achieved. On the other hand, the electron mobility achieved in this work is close to those reported (300–600 cm^2/V s) in metal-polar structures on AlN (red empty circles) with similar electron densities.[28–31]

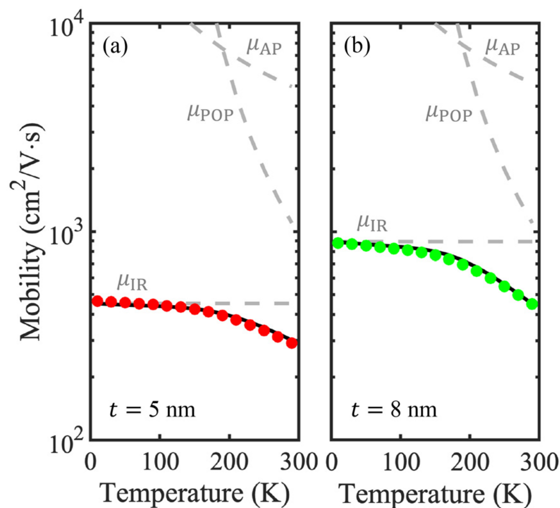

FIG. 4. Measured (circles) and calculated (black lines) electron mobility as a function of temperature for (a) 5 nm and (b) 8 nm GaN channels. Gray dashed lines show individual contributions from interface roughness scattering (μ_{IR}), acoustic phonon scattering (μ_{AP}), and optical phonon scattering (μ_{POP}).

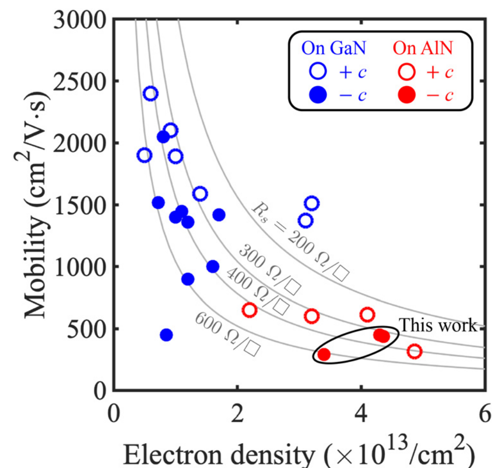

FIG. 5. Room temperature electron density and mobility reported in various 2DEG-inducing III-nitride semiconductor heterostructures. Empty symbols represent data from metal-polar (+c) AlGaN/GaN,[22–24] AlGaN/AlN/GaN,[25] and AlN/GaN[26,27] structures on GaN (blue) and AlN/GaN[28–31] structures on AlN (red). Filled symbols are data from N-polar (−c) GaN/AlGaN,[32,33] GaN/AlN/AlGaN,[19] and GaN/AlN digital alloy[17] structures on GaN (blue) and GaN/AlGaN structures on AlN in this work (red).

Published under an exclusive license by AIP Publishing

In summary, we report the observation of the unexplored polarization-induced 2DEGs in undoped pseudomorphic N-polar GaN/AlGaN heterostructures on N-polar single-crystal AlN substrates with smooth surface morphology and sharp hetero-interfaces by plasma-assisted MBE. The presence of high-density polarization-induced 2DEGs, which maintain down to cryogenic temperatures, was confirmed by temperature dependent Hall-effect measurements on multiple samples with varying GaN thicknesses. A combination of high electron density $>4\times10^{13}/\text{cm}^2$ and room temperature electron mobility $>430\,\text{cm}^2/\text{V s}$ leads to a low sheet resistance $\sim320\ \Omega/\square$ in samples with 8 and 10 nm GaN channels. A decrease in electron mobility was observed when GaN thickness was reduced to 5 nm. These results shed light on carrier transport in the high-density polarization-induced 2DEGs in N-polar GaN/AlGaN heterostructures strained to AlN and offer significant hope toward next-generation high-power RF electronics that take advantage of the high electrical resistivity and thermal conductivity of the AlN platform.

See the supplementary material for the material parameters used for energy band diagram simulation and mobility calculations.

The authors at Cornell University acknowledge financial support from Asahi Kasei, the Cornell Center for Materials Research (CCMR)—a NSF MRSEC program (No. DMR-1719875); ULTRA, an Energy Frontier Research Center funded by the U.S. Department of Energy (DOE), Office of Science, Basic Energy Sciences (BES), under Award No. DE-SC0021230; and AFOSR under Grant No. FA9550-20-1-0148. This work uses the CESI Shared Facilities partly sponsored by NSF No. MRI DMR-1631282 and Kavli Institute at Cornell (KIC).

AUTHOR DECLARATIONS

Conflict of Interest

The authors have no conflicts to disclose.

Author Contributions

Zexuan Zhang: Conceptualization (lead); Investigation (lead); Methodology (lead); Validation (lead); Writing – original draft (lead). **Jimy Encomendero:** Conceptualization (supporting); Investigation (supporting); Methodology (supporting); Validation (supporting). **Eungkyun Kim:** Conceptualization (supporting); Investigation (supporting); Methodology (supporting); Validation (supporting); Writing – review and editing (supporting). **Jashan Singhal:** Conceptualization (supporting); Investigation (supporting); Methodology (supporting); Validation (supporting); Writing – review and editing (supporting). **Yong Jin Cho:** Conceptualization (supporting); Investigation (supporting); Methodology (supporting); Validation (supporting); Writing – review and editing (supporting). **Kazuki Nomoto:** Conceptualization (supporting); Investigation (supporting); Methodology (supporting); Validation (supporting). **Masato Toita:** Funding acquisition (lead); Project administration (lead); Resources (lead). **Huili Grace Xing:** Conceptualization (lead); Funding acquisition (lead); Investigation (supporting); Methodology (supporting); Project administration (lead); Resources (lead); Supervision (lead); Validation (supporting). **Debdeep Jena:** Conceptualization (lead); Funding acquisition (lead); Investigation (supporting); Methodology (supporting); Project administration (lead); Resources (lead); Supervision (lead); Validation (supporting); Writing – review and editing (lead).

DATA AVAILABILITY

The data that support the findings of this study are available from the corresponding author upon reasonable request.

REFERENCES

[1] R. Chaudhuri, S. J. Bader, Z. Chen, D. A. Muller, H. G. Xing, and D. Jena, Science **365**, 1454 (2019).
[2] Z. Zhang, J. Encomendero, R. Chaudhuri, Y. Cho, V. Protasenko, K. Nomoto, K. Lee, M. Toita, H. G. Xing, and D. Jena, Appl. Phys. Lett. **119**, 162104 (2021).
[3] K. Nomoto, R. Chaudhuri, S. Bader, L. Li, A. Hickman, S. Huang, H. Lee, T. Maeda, H. Then, M. Radosavljevic *et al.*, in *2020 IEEE International Electron Devices Meeting (IEDM)* (IEEE, 2020), p. 8-3.
[4] G. Alvarez-Escalante, R. Page, R. Hu, H. G. Xing, D. Jena, and Z. Tian, APL Mater. **10**, 011115 (2022).
[5] M. H. Wong, Y. Pei, T. Palacios, L. Shen, A. Chakraborty, L. S. McCarthy, S. Keller, S. P. DenBaars, J. S. Speck, and U. K. Mishra, Appl. Phys. Lett. **91**, 232103 (2007).
[6] M. H. Wong, Y. Pei, R. Chu, S. Rajan, B. L. Swenson, D. F. Brown, S. Keller, S. P. DenBaars, J. S. Speck, and U. K. Mishra, IEEE Electron Device Lett. **29**, 1101 (2008).
[7] R. Kirste, S. Mita, L. Hussey, M. P. Hoffmann, W. Guo, I. Bryan, Z. Bryan, J. Tweedie, J. Xie, M. Gerhold *et al.*, Appl. Phys. Lett. **102**, 181913 (2013).
[8] Z. Zhang, M. Kushimoto, T. Sakai, N. Sugiyama, L. J. Schowalter, C. Sasaoka, and H. Amano, Appl. Phys. Express **12**, 124003 (2019).
[9] Y. Cho, C. S. Chang, K. Lee, M. Gong, K. Nomoto, M. Toita, L. J. Schowalter, D. A. Muller, D. Jena, and H. G. Xing, Appl. Phys. Lett. **116**, 172106 (2020).
[10] K. Lee, Y. Cho, L. J. Schowalter, M. Toita, H. G. Xing, and D. Jena, Appl. Phys. Lett. **116**, 262102 (2020).
[11] Z. Zhang, Y. Hayashi, T. Tohei, A. Sakai, V. Protasenko, J. Singhal, H. Miyake, H. G. Xing, D. Jena, and Y. Cho, arXiv:2204.08604 (2022).
[12] J. Singhal, J. Encomendero, Y. Cho, L. V. Deurzen, Z. Zhang, K. Nomoto, M. Toita, H. G. Xing, and D. Jena, arXiv:2206.11370 (2022).
[13] K. Lee, R. Page, V. Protasenko, L. J. Schowalter, M. Toita, H. G. Xing, and D. Jena, Appl. Phys. Lett. **118**, 092101 (2021).
[14] A. Smith, R. Feenstra, D. Greve, J. Neugebauer, and J. Northrup, Phys. Rev. Lett. **79**, 3934 (1997).
[15] A. Smith, R. Feenstra, D. Greve, M. Shin, M. Skowronski, J. Neugebauer, and J. Northrup, J. Vac. Sci. Technol. B **16**, 2242 (1998).
[16] Ł. Janicki, J. Misiewicz, M. Siekacz, H. Turski, J. Moneta, S. Gorantla, C. Skierbiszewski, and R. Kudrawiec, Sens. Actuators, B **281**, 561 (2019).
[17] S. Diez, S. Mohanty, C. Kurdak, and E. Ahmadi, Appl. Phys. Lett. **117**, 042102 (2020).
[18] H. Li, S. Wienecke, B. Romanczyk, E. Ahmadi, M. Guidry, X. Zheng, S. Keller, and U. K. Mishra, Appl. Phys. Lett. **112**, 073501 (2018).
[19] U. Singisetti, M. H. Wong, and U. K. Mishra, Appl. Phys. Lett. **101**, 012101 (2012).
[20] P. Sohi, D. Martin, and N. Grandjean, Semicond. Sci. Technol. **32**, 075010 (2017).
[21] R. K. Jana and D. Jena, Appl. Phys. Lett. **99**, 012104 (2011).
[22] C. Skierbiszewski, K. Dybko, W. Knap, M. Siekacz, W. Krupczyński, G. Nowak, M. Boćkowski, J. Łusakowski, Z. Wasilewski, D. Maude *et al.*, Appl. Phys. Lett. **86**, 102106 (2005).
[23] R. Gaska, M. Shur, A. Bykhovski, A. Orlov, and G. Snider, Appl. Phys. Lett. **74**, 287 (1999).
[24] Y. Cho, Y. Ren, H. G. Xing, and D. Jena, Appl. Phys. Express **12**, 121003 (2019).
[25] S. Elhamri, W. Mitchel, W. Mitchell, G. Landis, R. Berney, and A. Saxler, Appl. Phys. Lett. **90**, 042112 (2007).
[26] Y. Cao, K. Wang, A. Orlov, H. Xing, and D. Jena, Appl. Phys. Lett. **92**, 152112 (2008).
[27] Y. Cao, K. Wang, G. Li, T. Kosel, H. Xing, and D. Jena, J. Cryst. Growth **323**, 529 (2011).

Published under an exclusive license by AIP Publishing

[28]M. Qi, G. Li, S. Ganguly, P. Zhao, X. Yan, J. Verma, B. Song, M. Zhu, K. Nomoto, H. Xing *et al.*, Appl. Phys. Lett. **110**, 063501 (2017).
[29]R. Chaudhuri, A. Hickman, J. Singhal, J. Casamento, H. G. Xing, and D. Jena, Phys. Status Solidi A **219**, 2100452 (2022).
[30]S. Patwal, M. Agrawal, K. Radhakrishnan, T. L. A. Seah, and N. Dharmarasu, Phys. Status Solidi A **217**, 1900818 (2020).
[31]A. Hickman, R. Chaudhuri, S. J. Bader, K. Nomoto, K. Lee, H. G. Xing, and D. Jena, IEEE Electron Device Lett. **40**, 1293 (2019).
[32]S. Keller, C. Suh, N. Fichtenbaum, M. Furukawa, R. Chu, Z. Chen, K. Vijayraghavan, S. Rajan, S. DenBaars, J. Speck *et al.*, J. Appl. Phys. **104**, 093510 (2008).
[33]S. Rajan, A. Chini, M. H. Wong, J. S. Speck, and U. K. Mishra, J. Appl. Phys. **102**, 044501 (2007).
[34]Y. Cao and D. Jena, Appl. Phys. Lett. **90**, 182112 (2007).
[35]Y. Zhang, I. Smorchkova, C. Elsass, S. Keller, J. P. Ibbetson, S. Denbaars, U. K. Mishra, and J. Singh, J. Appl. Phys. **87**, 7981 (2000).

Published under an exclusive license by AIP Publishing